Environmental Science Processes & Impacts

PAPER

View Article Online
View Journal | View Issue

Cite this: *Environ. Sci.: Processes Impacts*, 2019, **21**, 845

Effect of maturity and mineralogy on fluid-rock reactions in the Marcellus Shale

John Pilewski,[a] Shikha Sharma, *[a] Vikas Agrawal,[a] J. Alexandra Hakala[b] and Mengling Y. Stuckman[b]

Natural gas extraction from the Appalachian Basin has significantly increased in the past decade. The push to properly dispose, reuse, or recycle the large amounts of produced fluids associated with hydraulic fracturing operations and design better fracturing fluids has necessitated a better understanding of the subsurface chemical reactions taking place during hydrocarbon extraction. Using autoclave reactors, this study mimics the conditions of deep subsurface shale reservoirs to observe the chemical evolution of fluids during the shut-in phase of hydraulic fracturing (HF), a period when hydraulic fracturing fluids (HFFs) remain confined in the reservoir. The experiment was conducted by combining a synthetic hydraulic fracturing fluid and powdered shale core samples in high temperature/pressure static autoclave reactors for 14 days. Shale samples of varying maturity and mineralogy were used to assess the effect of these variations on the proliferation of inorganic ions and low molecular weight volatile organic compounds (VOCs), mainly benzene, toluene, ethylbenzene and xylenes (BTEX) and monosubstituted carboxylic acids. Ion chromatography results indicate that the relative abundance of ions present was similar to that of water produced from HF operations in the Marcellus Shale basin. There was an increase of SO_4^{2-} and PO_4^{3-} and a decrease in Ba^{2+} upon fluid-shale reaction. Major ionic shifts indicate calcite dissolution in two of the fluid-shale reactions and barite precipitation in all fluid-shale reactions. Toluene, xylene, and carboxylic acids were produced in the shale-free control experiment. The most substantial increase in BTEX analytes was observed in reactions with low maturity shale, while the high maturity shale reaction produced no measurable BTEX compounds. Total organic carbon decreased in all reactions including fracturing fluid and shale, suggesting adsorption onto the organic matter (OM) matrix. The results from this study highlight that both the nature of OM and mineralogy play a key role in determining the fate of inorganic and organic compounds during fluid–shale interactions in the subsurface shale reservoir. Overall this study aims to contribute to the growing understanding of complex chemical interactions that occur in the shale reservoirs during HF, which is vital for determining the potential environmental impacts of HF and designing more efficient HFF and produced water recycling techniques for environmentally conscious natural gas production.

Received 28th September 2018
Accepted 15th February 2019

DOI: 10.1039/c8em00452h

rsc.li/espi

Environmental significance

Natural gas extraction from the Appalachian Basin has significantly increased in the past decade. The push to properly dispose, reuse, or recycle the large amounts of produced fluids associated with hydraulic fracturing operations and design better fracturing fluids has necessitated a better understanding of the subsurface chemical reactions taking place during hydrocarbon extraction. This study reports the results of laboratory experiments conducted to understand the effect of varying maturity and mineralogy of shale on the proliferation of inorganic ions and low molecular weight organic compounds, mainly benzene, toluene, ethylene, and xylene (BTEX) and monosubstituted carboxylic acids, in the reservoir after injection of hydraulic fracturing fluids.

1 Introduction

The Marcellus Shale is the largest natural gas producing reservoir in the United States, and over the past decade, the amount of natural gas extracted from the reservoir has almost tripled due to advancements in horizontal drilling technologies.[1] As a result, thousands of wells have been drilled in areas of Pennsylvania, Ohio and West Virginia, where most of the reservoir is underlain. Hydraulic fracturing is applied to stimulate production from tight reservoirs and involves the injection of millions of gallons of fluid (hydraulic fracturing fluid, HFF), which is composed of water, sand, and chemical additives.[2,3] The injected HFF is known to react with the reservoir rocks, resulting in changes in reservoir porosity and permeability due

[a]*West Virginia University Department of Geology & Geography, 330 Brooks Hall, 98 Beechurst Ave., Morgantown, WV 26506, USA. E-mail: shikha.sharma@mail.wvu.edu; Tel: +1-304-293-6717*

[b]*National Energy Technology Laboratory, U. S. Department of Energy, Pittsburgh, PA 15236, USA*

to HFF–mineral interactions.[4–7] These reactions also affect the chemistry of fluids produced from the formation.[8,9] Therefore, these interactions can affect both long-term hydrocarbon productivity from shale reservoirs and produced fluid treatment and management strategies. One area of study that requires further investigation is understanding the effect of HFF–shale reactions on the potential release of organic constituents, such as BTEX compounds, into the fluids produced from the reservoir. Additionally, understanding the role of thermal maturity and mineralogy is needed to improve the efficiency of fracturing treatments and the efficacy of produced fluid management. The overall outcome would be a reduced environmental footprint of hydrocarbon production from unconventional reservoirs.

The composition of fluids produced from both active wells and laboratory-based experiments differed from that of the initial injection fluid in prior studies, indicating that reservoir reactions and fluid mixing may both contribute significantly to the produced water chemical signatures.[8–11] Water produced from unconventional reservoirs is typically characterized by its relatively high total dissolved solids (TDS), varying concentrations of dissolved organic carbon (DOC), and sometimes an abundance of radioactive elements.[4,12,13] Monocyclic aromatic hydrocarbons such as benzene, toluene, ethylbenzene, xylene, and low molecular weight organic acids represent common soluble organic compounds observed in produced water.[3,14–16] Determining the source of soluble organic compounds is particularly challenging due to variations in organic additives used in different wells and the difference in organic matter throughout different maturity zones of the Marcellus Shale.[17] Identifying the sources of organic carbon and its evolution throughout the HF process is crucial for designing additives for HFF and ensuring proper disposal and handling at the surface after it has interacted with the organic-rich shale in the reservoir.

Hydraulic fracturing fluid (HFF) is composed of three main ingredients: 95% fresh water, 4% proppant or silica sand, and 1% chemical additives by wt%.[18] Although chemical additives constitute only 1% of the total fluid injected, at volumes of 3–4 million gallons of injected fluid per well,[18] this can result in 30 000 to 40 000 gallons of injected chemical additives. In the initial stages of fracturing, the friction of HFF must be lowered *via* friction reducing organic additives such as WFR-61LA,[2] which contains petroleum distillates and ethoxylated alcohols. Gelling agents are included in order to increase the HFF viscosity to transport the proppant into the induced fractures, which produces a linked 3D polymer structure with the addition of cross linkers such as boric acid and ethanolamine. Breaker compounds, such as ammonium persulfate, are included in the HFF mixture to subsequently react with the proppant transport gel to reduce the HFF viscosity for flowback. The breaker compounds are often included with the overall HFF mixture. However, they are expected to become reactive after a period of time or under certain reservoir conditions. For example, ammonium persulfate creates SO_4^{2-} free radical ions to break down the gel at elevated temperatures above 50 °C.[15,16,19]

The Marcellus Shale is characterized by its low permeability and high concentrations of total organic carbon (TOC).[1] The reservoir varies in depth longitudinally, increasing from 3000 ft in the northwest to 8000 ft in the southeastern portion of the reservoir. This variation in depth results in different maturity windows throughout the reservoir ranging from 0.5% R_0 (percentage of vitrinite reflectance) at shallower depths up to 3.5% R_0 in the deepest zones of the reservoir.[1] Gas-rich, over mature zones of the Marcellus contain type II-III kerogen that has been thermally altered, providing a predominantly aromatic chemical signature.[20–23] Less mature zones have similar type II–III kerogen, but it has not been thermally degraded or altered to the same extent, resulting in a relatively more aliphatic chemical signature.[21,24] It is possible that the shallow, less mature zones of the Marcellus Shale contain aliphatic chemical structures that serve as the source of labile organic compounds released during the well shut-in period.

Variations in shale mineralogy may also affect the reactivity of both organic additives in the HFF and the shale kerogen. The Marcellus Shale is composed of mostly mixed-layer clays, quartz, feldspar, calcite, and pyrite.[1] Relative abundances of these minerals can vary from zone to zone and can control the system's buffering capacity and alteration of organic materials. Previous fluid-rock reaction studies conducted at ambient pressure showed that the mineralogy of the shale, especially calcite and pyrite contents, controls the precipitation of iron-bearing minerals, removal/release of metal contaminants, evolution of fluid composition and porosity destruction or development.[5,6] Calcite rich shales possess high pH buffering capacity, which favors pyrite dissolution, the release and oxidation of Fe^{2+} ions and formation of Fe(III)-bearing precipitates.[5,6] These studies also showed that calcite and pyrite dissolution can cause the release of metal contaminants, whereas Fe-(oxy)hydroxide precipitation leads to removal of metal contaminants from solution. A recent study[25] showed that fracturing fluid interactions can also lead to significant changes in carbonyl content, aromaticity, average aliphatic chain length and release of metals from kerogen isolates. Although these studies provide a preliminary understanding of inorganic and organic reactions that might take place during shale-fracturing fluid interactions, they were performed under ambient pressure conditions as opposed to *in situ* reservoir pressure conditions.

The objective of this study is to perform laboratory experiments to effectively simulate fluid-shale reactions under *in situ* high pressure/temperature reservoir conditions and to elucidate the fate of inorganic and organic reactants and products from HF operations within different maturity zones of a reservoir. To our knowledge, this is one of the first studies that has tried to compare shale–fluid interactions in shale samples collected from a range of maturity and mineralogy within a single shale basin. Determining the downhole chemical evolution of the fluid used to fracture the Marcellus Shale is critical for improving hydrocarbon recovery from tight shales and identifying effective water treatment and management strategies for produced fluids.

2 Materials and methods

Fluid–shale reactions were conducted using Parr 4768 static autoclaves to mimic and analyze the *in situ* fluid–shale reactions during the shut-in phase of hydraulic fracturing. The specific analyses focused on the major changes of inorganic ions and the proliferation of low molecular weight organic compounds within the fluid.

2.1 Sampling and preparation

The fluid used in the reaction vessels was a mixture of synthetic formation brine and synthetic HFF, prepared per methods reported for core flood experiments simulating the shut-in period of a Marcellus Shale HF operation, as reported[4] (Table 1). Three shale samples of varying maturity were collected from Marcellus Shale cores from different depths and geographical zones of the reservoir (Table 2). All samples have TOC values greater than 9 wt%, and OM sourced from mixed marine and terrestrial sources, representing type II-III kerogen.[20,21,26] The maturity of the samples is represented as percent vitrinite reflectance (% R_0). The % R_0 is calculated directly from the T_{max}, a thermal maturity parameter determined by pyrolysis analysis, which is the temperature where the hydrocarbon generation rate from kerogen peaks.[27] Mineralogy was analyzed as part of this study (Table 2) and is further described in both the Methods and Results sections. To prepare shale samples for static autoclave reactions, core samples were first washed using deionized water to avoid contamination from drill mud and then crushed using a SPEX mixer mill to a 100 mesh powder to maximize surface area and enhance reaction kinetics.

Table 1 The chemical composition of the synthetic HFF and brine mixture used for experiments in this study (see ref. 4)

Composition of Hydraulic Fracturing Fluid (HFF)		
Ingredient	Purpose	Concentration weight%
Deionized water	Carrier fluid	99.36%
Hydrochloric acid	Perforation cleaner	0.25%
WGA-15L	Gelling agent	0.15%
WCS-631LC	Clay stabilizer	0.106%
WFR-61LA	Friction reducer	0.049%
Ammonium persulfate	Breaker	0.020%
Glutaraldehyde	Biocide	0.019%
Potassium hydroxide	pH adjuster	0.014%
Potassium carbonate	pH adjuster	0.012%
Ethylene glycol	Scale inhibitor	0.0045%
Citric acid	Iron control	0.0034%
Boric acid	Cross linker	0.0020%
Ethanolamine	Cross linker	0.0014%
WAI-251LC	Corrosion inhibitor	0.0013%
Composition of brine		
Ingredient		Concentration weight%
Deionized water		97.12%
Boric acid		0.002%
Potassium carbonate		0.024%
Barium chloride dehydrate		0.046%
Potassium chloride		0.022%
Strontium chloride sesquihydrate		0.14%
Ammonium chloride		0.016%
Sodium bromide		0.018%
Calcium chloride dehydrate		0.74%
Magnesium chloride sesquihydrate		0.19%
Sodium chloride		1.67%
Sodium sulfate		0.0002%
Sodium bicarbonate		0.015%

2.2 Experimental design

To emulate reservoir conditions during the shut-in phase, experiments were conducted using two 4768 Parr Instrument Company 600 mL high-temperature/pressure vessels set to ~2500 psi and 100 °C respectively. These values were used to best mimic *in situ* reservoir conditions of the Marcellus Shale while remaining within the limitations of the vessels.[4,8] Inside each 600 mL pressure vessel, a small Teflon cup was placed containing a fixed HFF–shale ratio (20 : 1) of 400 mL of fluid and 20 g of shale, following a previous study.[8] The remaining volume of each vessel was then filled with pressurized, inert N_2 (100% pure) to 2500 psi. Four experiments were conducted, each for 14 days to mimic an intermediate-term shut-in phase of an HF operation.[4] One experiment only contained HFF (no shale), and the other three experiments were performed with both HFF and the three shale samples described above. Fluids and shale were mixed immediately prior to pressurizing the reactors. Duplicate experiments were not performed due to limitations in the availability of shale samples.

2.3 Analytical methods

Five fluid samples were collected and analyzed in this study: NR-HFF (Non-Reacted Hydraulic Fracturing Fluid: the original fracturing fluid synthesized for this study), which served as a control and HPT-HFF (High Pressure/Temperature Hydraulic Fracturing Fluid: HFF exposed to high pressure and temperature in the absence of shale) and LM-2, WV-7, and MIP-3H fluids collected after the fluid–shale reactions with respective shale samples.

Fluid samples were collected from the reactors at the conclusion of the 14 day experiment using a high-density polyethylene Luer syringe and filtered *via* a 0.45 μm Whatman™ syringe filter attachment. Samples for ion chromatography (IC, ThermoFisher ICS-5000+ with AS11-HC column for anion and CS16 column for cation quantification) were collected with minimal headspace in 10 mL plastic vials. IC analysis focused on observing low molecular weight monosubstituted carboxylic acids (*e.g.*, acetate, formate, butyrate, and succinate) and dissolved major cations and anions of interest in this study (*e.g.*, Ba^{2+}, SO_4^{2-}, and PO_4^{3-}). All the samples were run in triplicate, and the standard error of IC measurements reported here was generally less than ± 3%. Additionally, every 10–20 samples, a cation/anion control sample (Sigma Aldrich, Inc.) was added during measurements,

Table 2 Organic and mineral composition of three shale samples from Marcellus Shale cores, collected from three different depths and geographical areas. The % R_0 and TOC values were reported by previous studies (see ref. 20 and 21). Semi-quantitative XRD data are used for LM-2, WV-7, and MIP-3H samples analyzed in this study

Sample id	Depth (ft)	% R_0	T_{max} (°C)	TOC (wt%)	Quartz (wt%)	Calcite (wt%)	Dolomite (wt%)	Pyrite (wt%)	Mixed clays (wt%)
LM-2	5825.7	0.8	443	15.4	28	21	5	5	42
WV-7	6615.8	1.4	475	12.9	23	ND	4	2	71
MIP-3H	7511.8	2.9	561	9.0	46	16	5	11	22

Table 3 Cation and anion concentrations in fluid samples in mg L^{-1} measured *via* IC. Also included is the pH for each fluid sample and overall total dissolved solids (TDS in mg L^{-1}). For dissolved inorganic carbon (DIC), values are either not detected (ND) or reported in mg as C/L. The values reported are the average of samples run in triplicate and the standard error of all measurements is < ± 3%

	pH	F^-	Br^-	NO_3^-	SO_4^{2-}	PO_4^{3-}	Cl^-	Li^+	Na^+	NH_4^+	K^+	Mg^{2+}	Ca^{2+}	Sr^{2+}	Ba^{2+}	DIC
Det. limit	—	0.04	0.26	0.2	0.5	0.4	0.2	0.04	0.4	0.2	0.2	0.2	0.4	0.1	0.1	0.5
NR-HFF	1.3	0.6	107	4.5	9.6	ND	16 729	ND	6583	89	393	213	2015	464	96	ND
HPT-HFF	1.9	0.5	60	2.3	10.6	ND	7809	ND	3277	52	165	104	967	224	39	ND
LM-2	6.1	3.2	68	1.7	189.8	6.8	9060	0.1	3727	51	205	132	1606	211	4	35.2
WV-7	2.3	9.9	110	5.1	271.5	29.8	16 867	0.2	6663	92	427	418	2576	367	ND	ND
MIP-3H	5.7	3.6	65	1.6	66.1	9.6	8894	0.2	3673	50	202	165	1418	228	11	15.8

whose accuracy is within 95–105%. The detection limits for the organic acids and ions analyzed in this study are indicated in Table 3 and Table 4.

Sample splits for non-purgeable organic carbon (NPOC) and dissolved inorganic carbon (DIC) were analyzed with a Shimadzu Total Organic Carbon/Total Inorganic Carbon (TOC/TIC) analyzer. Average values from 3–5 replicates were reported with <2% precision (% RSD), and quality control samples for every 10–12 samples demonstrated consistent accuracy within 95–105%.

Volatile organic carbon (VOC) analytes were sampled in accordance with the methods described in Chapter 4 of *EPA SW-486 Compendium: Organic Analytes*. Samples for VOC analysis were placed in pre-cleaned 60 mL volatile organic analysis (VOA) vials and acidified with minimal headspace to preserve target analytes. VOCs were efficiently transferred from the aqueous phase to the vapor phase by bubbling helium at a flow rate of 40 mL min^{-1} through a portion of the aqueous sample at ambient temperature and purged for 11 minutes. The vapor was swept through a sorbent trap (Supelco Trap A, Tenax 24 cm) where the volatile components were adsorbed. The sorbent trap was then heated at 180 °C for 12 minutes and backflushed with an inert gas to desorb the components onto a gas chromatographic (GC) column (30 m × 0.53 mm ID VOCOL capillary column with 3 μm film thickness). A temperature program of 2 °C min^{-1} to 75 °C (with initial temperature of 45 °C) then 25 °C min^{-1} to 220 °C and hold 2 minutes was used in the gas chromatograph (GC) to separate the organic compounds. A photo-ionization detector (PID) was used for detection of the aromatic compounds. This analysis was performed at REIC Labs in Morgantown, WV, within one day of sampling, and the samples were kept at 4 °C until analyzed. The analysis was conducted in accordance with EPA Method 8260B and analytes of focus included benzene, toluene, ethylbenzene and xylene with a detection limit of 1 μg mL^{-1} for benzene, toluene, ethylbenzene, and *o*-xylene and 2 μg mL^{-1} for *m*/*p* xylene.

Mineral compositional analysis was performed on powdered shale samples (using SPEX mixer mill) using a PANalytical X'Pert Pro X-ray diffractometer with a CuKα source at 2θ angles from 5° to 75° and a step time of ~12 s per degree (total scan time 13.5 min). A 20 mm slit was used to focus X-rays onto an Xcelerator™ detector. Samples were

Table 4 Dissolved organic carbon (DOC) concentrations in fluid samples in mg L^{-1}, where NPOC = non-purgeable organic carbon in mg as C/L and volatile organic carbon (VOC) concentrations in μg L^{-1}, for each fluid sample. The values reported are the average of samples run in triplicate and within 2% precision (% RSD)

	DOC concentrations in mg L^{-1}					VOC concentrations in mg L^{-1}			
Sample id	NPOC	Acetate	Formate	Butyrate	Succinate	Benzene	Toluene	*m*,*p*-Xylene	*o*-Xylene
Det. limit	1.0	0.1	0.1	0.18	0.1	1.0	1.0	2.0	1.0
NR-HFF	243	ND	6.1	ND	1.9	ND	ND	ND	ND
HPT-HFF	317	19.3	13.9	1.6	1.0	0.0	2.7	5.9	3.8
LM-2	264	12.5	10.2	3.0	0.9	2.5	14.8	10.2	5.6
WV-7	197	16.3	6.9	1.7	3.0	ND	1.3	4.7	2.4
MIP-3H	235	12.7	9.4	2.3	1.1	ND	ND	ND	ND

irradiated on a spinning stage (1 rps), with anti-scatter and divergence slit angles of 1° and 0.5°, respectively. The X-ray beam was operated at a current of 40 mA and a voltage of 45 kV. Spectra were interpreted using the X'pert HighScore Plus Program to evaluate the percentage of various mineral phases present. Semi-quantitative estimation of percentages was performed using the reference-intensity ratio (RIR) matrix-flushing method[28,29] based on selected PDF2 reference samples chosen for each mineral phase. The wt% of minerals was calculated to the nearest unit, and the total sum of the minerals was within 100 ± 1 wt%.

Geochemical modeling of the IC and DIC data for each fluid (NR-HFF, HPT-HFF, LM-2, WV-7, and MIP-3H) was performed using Geochemists Workbench Professional v. 10.0 using the MINTEQ database to calculate the saturation indices of minerals in the system (sulfate, carbonate, and phosphate bearing).

3 Results

3.1 Mineralogy and aqueous inorganic chemistry

The Marcellus Shale samples in this study were mixed layer clays with lower fractions of carbonate, quartz, pyrite, and feldspar as compared to clay minerals (Table 2), consistent with mineral compositions in previous studies.[30,31] Calcite abundance differed amongst the samples, in which it was identified in the LM-2 (21 wt%) and MIP-3H (16 wt%) samples, but it was not detected in the WV-7 sample (Fig. 1). Dolomite and pyrite were both detected within 1–10 wt% in all three shale samples (dolomite: LM-2 5 wt%, WV-7 4 wt%, and MIP-3H 5 wt%; pyrite: LM-2 and MIP-3H 5 wt%, and WV-7 2 wt%). Mixed clay and quartz contents varied amongst all samples (Table 2). No direct relationship was observed between mineralogy and thermal maturity (Fig. 1). However TOC decreased with increasing thermal maturity (Table 2).

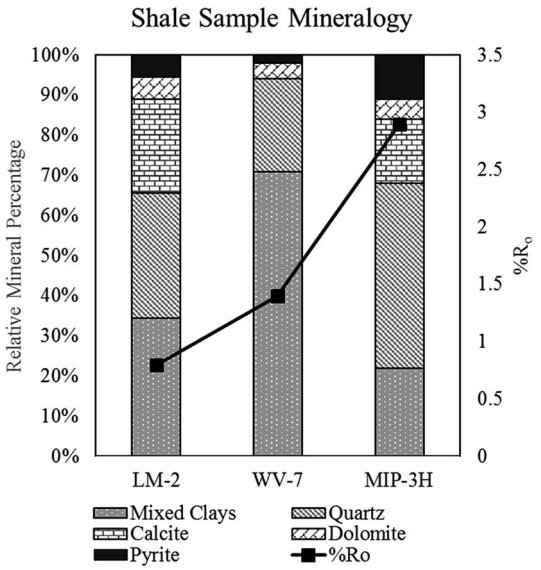

Fig. 1 Relative percentages of minerals in three shale samples overlain by their % R_0 (maturity) values.

The results indicate that except sulfate, almost all cations and anions are reduced by half on increasing pressure and temperature in shale-free fracturing fluids (HPT-HFF) as compared to the initial non-reacted NR-HFF (Table 3). However, the most measurable changes observed in IC-analyzed inorganic species are for shale-reacted fluids, where both SO_4^{2-} and PO_4^{3-} increased and Ba^{2+} decreased (Table 3 and Fig. 2). Sulfate concentrations in the shale-reacted samples were all elevated relative to that in the HPT-HFF sample, which is the shale-free control experiment (Table 3 and Fig. 2). The NR-HFF and HPT-HFF shale-free samples contained 9.6 mg L^{-1} SO_4^{2-} and 10.6 mg L^{-1} SO_4^{2-}, respectively. For experiments containing shale, SO_4^{2-} was 189.8 mg L^{-1} (LM-2), 271.5 mg L^{-1} (WV-7), and 66.1 (MIP-3H). Barium concentrations in the shale-reacted samples were either substantially lower (less by at least 70%) or non-detectable, relative to the shale-free control sample HPT-HFF (Table 3 and Fig. 2). All shale-reacted samples showed a substantial decrease in Ba^{2+} relative to the shale-free experiments ($[Ba^{2+}] = 3.8$ mg L^{-1} (LM-2), 10.6 mg L^{-1} (MIP-3H), and not detectable (WV-7)), while the shale-free samples contained $[Ba^{2+}] = 96.2$ mg L^{-1} (NR-HFF) and 39.1 mg L^{-1} (HPT-HFF). No measurable PO_4^{3-} was present in NR-HFF or HPT-HFF; however, it was detected in all shale-reacted fluids ($[PO_4^{3-}] = 6.9$ mg L^{-1} (LM-2), 29.8 mg L^{-1} (WV-7), and 9.6 mg L^{-1} (MIP-3H)) (Table 3 and Fig. 2). The pH values under shale-free conditions remained low, where the pH value of NR-HFF was 1.3 and that of HPT-HFF was 1.9. For the shale-reacted samples, the pH values varied and were measured to be 2.3 (WV-7), 5.73 (MIP-3H), and 6.07 (LM-2) (Table 3). Dissolved inorganic carbon was detected in only two samples, LM-2 and MIP-3H. LM-2 contained 35.18C mg L^{-1}. DIC and MIP-3H contained 15.8 mg L^{-1} DIC. The WV-7 fluid had no observable inorganic carbon (Table 3).

3.2 Aqueous organic chemistry

Substantial changes were observed in the organic chemistry of fluids collected from all experiments performed at elevated pressure and temperature compared to the shale-free control that remained under ambient conditions. Target volatile organic compounds (VOCs) were detected in the shale-free HPT-HFF sample (no shale, elevated *P* and *T*), which also contained

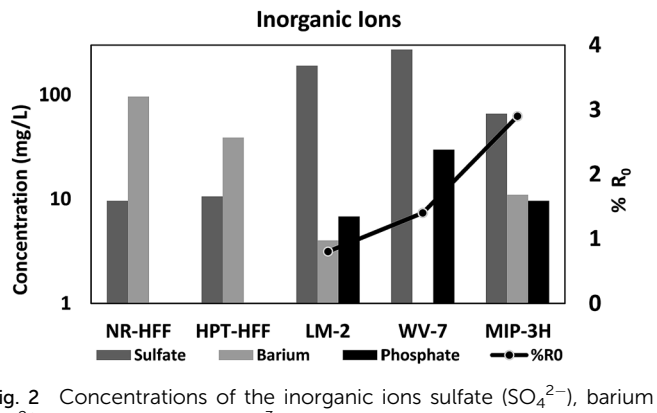

Fig. 2 Concentrations of the inorganic ions sulfate (SO_4^{2-}), barium (Ba^{2+}), and phosphate (PO_4^{-3}) in all fluid samples plotted against the thermal maturity of the reacted shale.

elevated non-purgeable organic carbon (NPOC) relative to the control NR-HFF fluid (no shale, ambient P and T) (Table 4). For experiments with shales of different thermal maturity, VOCs were detected at higher concentrations in the low-maturity shale (LM-2) relative to all other samples and at around the same levels for the intermediate-maturity shale (WV-7) as the HPT-HFF sample. VOCs were not detected in fluids from the experiment with the highest thermal maturity shale (MIP-3H) (Table 4 and Fig. 3A).

The target VOC analytes, BTEX compounds, were observed in HPT-HFF at relatively low concentrations. The HPT-HFF fluid contained toluene concentrations of 2.7 μg L^{-1} and xylene concentrations of 9.7 μg L^{-1}. The fluid from the LM-2 reaction was the only sample that contained benzene, at a concentration of 2.5 μg L^{-1}. The LM-2 sample also contained toluene (14.8 μg L^{-1}) and xylene (15.8 μg L^{-1}). The WV-7 fluid contained toluene (1.3 μg L^{-1}) and xylene (7.1 μg L^{-1}). HPT-HFF, WV-7 and LM-2 samples contained no measurable amount of ethylbenzene, and the fluid from the MIP-3H reaction produced no observable BTEX compounds. It is also important to note that NR-HFF had no measurable BTEX compounds (Table 4 and Fig. 3A).

No direct trend between fluid-phase NPOC and either the R_0 or the experimental P and T was observed (Table 4). The NPOC values were elevated in some experiments performed at elevated P and T (HPT-HFF > LM-2) relative to the shale-free ambient P and T fracturing fluid (NR-HFF); however, two experiments contained lower NPOC (NR-HFF > MIP-3H > WV-7) (Table 4). Low molecular weight organic acids (acetate, formate, butyrate, and succinate) were detected in all experimental fluids, and they were the highest in the HPT-HFF and lowest in NR-HFF (Table 4 and Fig. 3B). Fluids from the experiments containing shale contained different proportions of individual organic acids; however, the total values were similar across the three shale samples, and individual organic acids did not display any trends with thermal maturity (Table 4 and Fig. 3B).

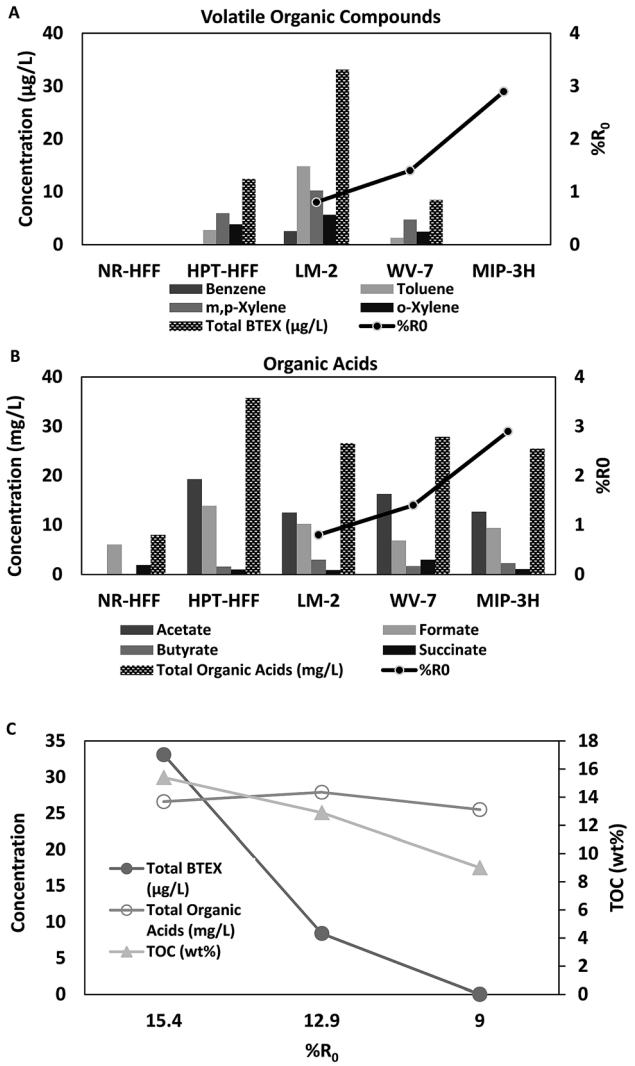

Fig. 3 (A) Volatile organic compound concentrations in all fluid samples plotted against the thermal maturity for the reacted shales. (B) Organic acid concentrations in all fluid samples plotted against the thermal maturity of the reacted shales. (C) Plot of the relationship between total target VOCs, total target organic acids, TOC, and % R_0. For panels A and B, the cross-hatched bar represents the sum of concentrations for each class of compounds measured in the sample. Components without bar display are not detectable (A and B). In panel C, the lines indicate the direction of the data trend and do not represent a calculated fit of the data.

4 Discussion

4.1 Inorganic mineral reactions affecting shale composition and produced fluid chemistry

The differences in the inorganic fluid chemistry between the five experimental fluids demonstrate that inorganic reactions occur both due to changes in P and T conditions and geochemical interactions between HFF and the shale. A net decrease (almost half) is observed in almost all cations (Na^+, K^+, Ba^{2+}, Sr^{2+}, Mg^{2+}, and Ca^{2+}) upon increasing the pressure and temperature of the shale-free HFF sample (comparison between NR-HFF and HPT-HFF is shown in Table 3). The observed change in inorganic ions (especially cations) could result from chelation with fracturing fluid additives or potential chemical transformation or precipitation during the experiment. Chelation of inorganic ions is possible due to the presence of ligands in scaling inhibitors and cross linkers (such as ethylene glycol or ethanolamine) in the fracturing fluid. For example, ethylene glycol is reported to form complexes with certain divalent metal halides.[32] Additionally, if anions such as Br^- transformed into BrO_3^- due to reaction with sulfate radicals,[33] present as a result of ammonium persulfate breakdown in our experiments, the resulting BrO_3^- anion would not be detectable with the IC method applied in this study. Further, changes in temperature may also have resulted in the formation of non-detected precipitates in the reactor, or removal of precipitates during fluid sampling and filtration.[34] Geochemical modeling was used to understand the evolution of inorganic species in the experiments. However, the changes observed in IC analysis between NR-HFF and HPT-HFF are not consistent with the predictions of the model (Table 5). This could be because geochemical modeling software does not account for the effect of processes like chelation and filtration on the fluid chemistry. Although

Table 5 Saturation indices for major and potential scale-forming minerals, as calculated in Geochemist's Workbench v. 10.0 using the MINTEQ database. The values are reported as log Q/K. Iron- and silica-bearing phases are not included as Fe and Si were not measured in fluids in this study. Blank values indicate that the mineral SI contained no value for that particular calculation

Mineral	Chemical formula	NR-HFF	HPT-HFF	LM-2	WV-7	MIP-3H
Barite	$BaSO_4$	1.09	1.06	1.35		1.34
Celestite	$SrSO_4$	−1.43	−1.37	−0.12	0.11	−0.53
Gypsum	$CaSO_4 \cdot 2H_2O$	−2.52	−2.44	−0.95	−0.77	−1.44
Calcite	$CaCO_3$			−0.82		−1.86
Strontianite	$SrCO_3$			−1.22		−2.17
Witherite	$BaCO_3$			−3.81		−4.36
FCO_3-apatite	$Ca_{10}(PO_4)_5(CO_3)F_3$			18.77		14.62
Fluorite	CaF_2	−3.69	−3.01	0.88	0.63	0.93
Hydroxyapatite	$Ca_5(PO_4)_3(OH)$			4.50	−19.41	2.21

the interaction of HFF with the wall of the reactor could occur, this is unlikely as the containers used to conduct the experiments were made of Teflon, which is not anticipated to affect the cationic composition of the fluids. There is a possibility of adsorption/desorption of organic molecules on/from the Teflon. However, the experimental conditions for all the reactions (with and without shale) were the same. Therefore, relative differences observed in the concentration of organic molecules between different experiments are most likely due to shale fracturing fluid interactions.

Reactions involving shale appear to be largely controlled by reactions involving carbonate minerals. The HFF formulation applied in this study included HCl and started with low pH (Table 1, Table 3), which is common for the HFF applied in the Marcellus Shale.[6] HCl is used for cleaning perforations prior to injecting fracturing fluid mixtures and is a common additive used to prevent scaling of secondary minerals.[18] The pH of LM-2 and MIP-3H fluid samples increased substantially (to 6.1 and 5.7, respectively; Table 3), indicating that carbonate minerals in these shale samples acted as effective buffers during the reaction, similar to prior observations.[4,5,8,35] The pH of our WV-7 sample remained low, with a similar value to the HPT-HFF (no-shale) experiment at elevated P and T, indicating the minimal buffering capacity of the WV-7 shale (Table 3).

The differences in the pH buffering capacity between the LM-2, MIP-3H, and WV-7 samples can be explained by differences in the calcite content between the samples, where LM-2 and MIP-3H contain 21 and 16 wt%, respectively, while calcite was not detected in WV-7 (Table 2 and Fig. 1). Calcite saturation indices calculated for our experimental fluids (only LM-2 and MIP-3H, as these were the only samples with detectable DIC as a calculation input) showed that both shale-reacted solutions were undersaturated with respect to calcite (Table 5). These results are consistent with other studies focused on HFF–shale reactions, which showed that the calcite content of the shale significantly controlled pH buffering and mineral dissolution and precipitation reactions.[4–6,8,35]

The potential for mineral scale formation involving barite was evaluated for our experiments, based on the changes in Ba^{2+} and SO_4^{2-} observed between the experiments with and without shale (Table 3 and Fig. 2). Application of the experimental data in geochemical equilibrium calculations showed that barite is supersaturated in all experimental fluids, except for the WV-7 experiment (Table 5). The only reason for this difference with WV-7 is because no Ba^{2+} was detected *via* IC for the fluid sample, which likely indicates that all Ba^{2+} in that experiment was removed *via* precipitation. Barite precipitation during HFF–shale interactions has been observed by various investigators,[4,7,36] has the potential to affect shale porosity and permeability,[4,7] and may play a role in shale oxidation–reduction.[8,37]

Multiple sources for Ba^{2+} and SO_4^{2-} exist in the HFF–shale reaction scenario. Although Ba^{2+} in unconventional reservoirs may originate from trapped drilling mud,[38] Ba^{2+} may also be present within the shale, release upon HFF–shale interaction under low pH conditions, and re-precipitate once carbonate mineral dissolution buffers the system pH.[7,9,37,38] Potential sources of SO_4^{2-} include fracturing fluid additives (*e.g.*, ammonium persulfate), sulfate-bearing minerals in the shale (*e.g.*, anhydrite), and oxidative dissolution of pyrite.[5,8,39] Previous studies postulate that due to the high buffering capacity of calcite, shale samples containing a higher content of calcite result in the higher dissolution of pyrite and higher concentration of SO_4^{2-}.[5,6]

In our study, it was observed that the WV-7 shale sample had the highest SO_4^{2-} concentration even though it contains the least amount of calcite and pyrite as compared to LM-2 and MIP-3H shale samples (Table 3 and Fig. 2). This is in contrast to conclusions made by previous studies.[5,6] We postulate that a large amount of sulfate formation in the WV-7 fracturing fluid experiments results from the more extensive breakdown of the ammonium persulfate breaker. This could possibly result from the presence of a higher clay content (almost double) in the WV-7 sample. The clay carries a net negative charge on its surface which can interact with the ammonium ion (NH_4^+) in the ammonium persulfate breaker. We postulate that association of NH_4^+ with negatively charged clay surfaces could enhance dissociation of ammonium persulfate. Higher breakdown of ammonium persulfate will release more sulfate ions into the solution. The higher sulfate concentration will also lead to the formation of a higher amount of the $BaSO_4$ precipitate by taking up free barium ions present in the solution. We postulate that this ultimately results in a greater decrease in barium ions in the WV-7 reacted fluid sample as

compared to LM-2 and MIP-3H reacted fluid samples (Fig. 2 and Table 3).

A new observation from the experiments performed in this study is the change in fluoride and phosphate concentrations in fluids from certain HFF–shale experiments and the subsequent supersaturation of certain PO_4^{3-}- and F^--bearing minerals (Tables 3 and 5). The absence of PO_4^{3-} in the NR-HFF and HPT-HFF and the increase in concentrations in all fluid samples are evidence that the F^- and PO_4^{3-} is leaching from the powdered shale (Table 3). The possible sources of F^- and PO_4^{3-} are apatite ($Ca_5(PO_4)_3(OH)$ and Ca_{10} $(PO_4)_5(CO_3)F_3$) and fluorite minerals present in shale samples (Table 5). Although these phases were not detected in XRD analysis probably because of their lower abundance in the samples, a prior study on Marcellus shale also detected evidence for authigenic apatite minerals such as carbonate fluorapatite using a phosphate-specific sequential extraction step.[40] The variations in concentrations of F^- and PO_4^{3-} in the fluid samples could possibly be due to the variations in concentrations of the F^- and PO_4^{3-} rich minerals in the shale and/or different Eh and pH conditions of the solution. The higher concentration of F^- and PO_4^{3-} in the fluid sample of WV-7 as compared to LM-2 and MIP-3H is likely due to the higher dissolution of F^- and PO_4^{3-} rich minerals present in the WV-7 shale sample as indicated by their lower saturation index values (Table 5). Geochemical equilibrium modeling showed that both LM-2 and MIP-3H fluids are supersaturated with respect to FCO_3-apatite and hydroxyapatite, while all three HFF–shale experiments are supersaturated with respect to fluorite (Table 5). Similar observations of apatite precipitation are reported for Huntersville Chert surfaces when exposed to Marcellus Shale produced water.[36] Formation of these precipitates can clog up the pore spaces during hydraulic fracturing operation and thus have implications on well productivity.

To evaluate how representative the experimental fluids from this study are to field-collected produced water from the Marcellus Shale, we compared the composition of our shale-reacted fluids with data reported for Marcellus produced water by the USGS.[41] Experimental values for our shale-reacted experiments (LM-2, MIP-3H, and WV-7) fall within the USGS-reported range of values (Fig. 4). The similarities observed in the mineral reactions between this and prior studies and in the reported produced water compositions from the Marcellus Shale indicate that the inorganic and organic reactions discussed in this and next section respectively are representative of the Marcellus Shale reservoir conditions.

4.2 Aqueous organic chemistry

Differences in organic chemistry between the NR-HFF, HPT-HFF, and experiments containing shale (LM-2, WV-7, and MIP-3H) indicate that the HFF reacts at elevated *P* and *T* both in the absence and presence of shale and that the shale controls the evolution of aqueous organic chemistry in the LM-2, WV-7 and MIP-3H experiments (Table 4 and Fig. 3).

Exposing HFF to elevated pressure and temperature resulted in differences in the total dissolved organic carbon (DOC) concentrations between the shale-free experiments (where DOC represents the non-purgeable organic carbon (NPOC) and

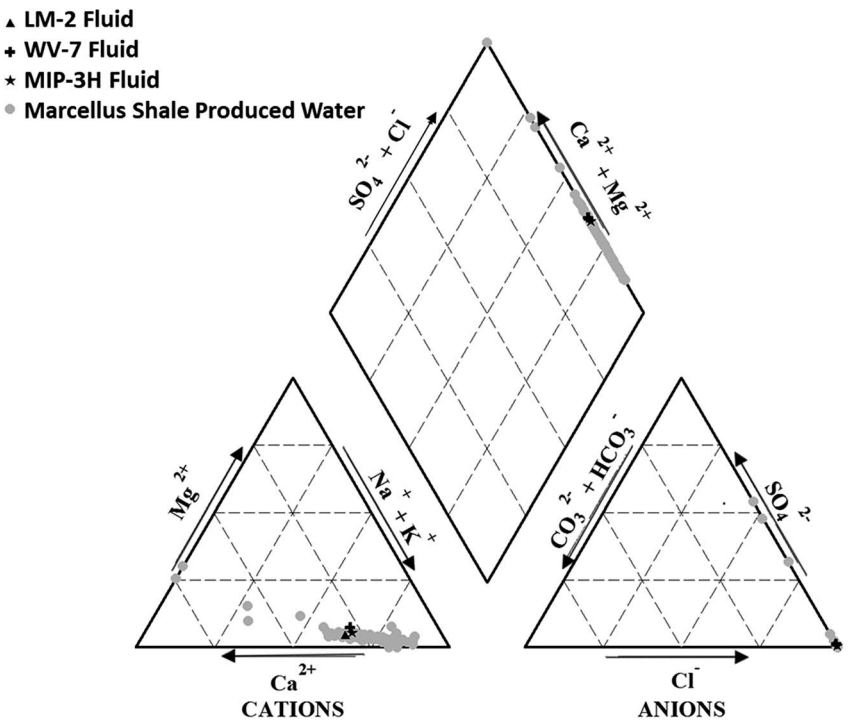

Fig. 4 Piper diagram showing the relative amounts of the most abundant ions in solution. Grey dots represent water produced from hydraulic fracturing operations in the Marcellus Shale basin collected by the USGS and the black markers overlain represent the three fluid samples from fluid–shale reactions in this study.

organic acids measured in the experimental fluids) and volatile organic compound (VOC) content (Table 4). The DOC increased for the HPT-HFF relative to the NR-HFF, which results from reactions involving the HFF additives. The combination of gelling agents and cross linker is applied during hydraulic fracturing to increase the molecular weight of the injected HFF in order to transport the proppant.[42] The cross linker may also link other components of the fracturing fluid, resulting in larger organic molecules that are rendered non-purgeable in the HPT-HFF. Boric acid and ethanolamine were both included in the HFF recipe used for this study, and boric acid is reported to catalyze multiple organic transformations.[43]

Increases in the organic acid and VOC content in the absence of shale show that both classes of compounds can be produced solely from HFF exposure to reservoir pressure and temperature conditions. Although formate and succinate are present in the NR-HFF solution, likely included as part of the HFF chemical additives (Table 1), in the HPT-HFF acetate and butyrate are measured above the detection limit, formate concentrations double, and succinate decreases (Table 4 and Fig. 3B). Toluene and xylenes are also generated upon exposure of HFF to reservoir conditions and are detectable in HPT-HFF (and below the detection limit in NR-HFF) (Table 4 and Fig. 3C). A prior study showed that certain organic additives, such as gelling and friction agents, degraded under reservoir conditions and were able to produce lower molecular weight organic compounds.[19]

The concentration and speciation of dissolved organic constituents differed in experiments containing shale (LM-2, WV-7, and MIP-3H) relative to the shale-free HFF reacted at elevated P and T (HPT-HFF). Experiments containing shale exhibited similarities in total organic acid concentrations across shale types. However, these organic acid concentrations were lower along with NPOC when compared to the HPT-HFF fluid (Table 4 and Fig. 3B). The shale OM matrix (kerogen) may act as a location for adsorption of the dissolved organic carbon (DOC: organic acids + NPOC) compounds onto the surface. More mature shale contains more aromatic compounds within its OM, resulting in higher organic porosity and relatively high surface area within this matrix.[44,45] This organic porosity creates an effective adsorbent trap for organic molecules used or generated in the hydraulic fracturing process.[45] Other laboratory fluid-shale studies observed a similar decrease in DOC in the fluid samples from autoclave reactions while also observing an increase in TOC in the solid sample.[8,19] Alternatively, components of the shale may catalyze the degradation of dissolved OM,[19,46] subsequently lowering the concentrations of organic acids and NPOC in the LM-2, WV-7, and MIP-3H experiments relative to the HPT-HFF experiment.

Although organic acid concentrations were lower in the experiments containing shale, it is possible that some of the organic acids released into the fluid were generated from the shale kerogen (as opposed to solely being sourced from the hydraulic fracturing fluid). Low molecular weight carboxylic acids, in particular, acetate and formate, have been observed in both produced water and fluids from similar fluid-shale experiments.[11,14,47] The proliferation of these compounds is considered to be related to the labile ester linked carboxyl functional groups attached to the OM within the shale formation. These labile functional groups are formed through the process of diagenesis[48] and are thought to be extracted from the shale reservoir upon hydraulic fracturing and fluid saturation.[47] Water-soluble organic acids have been measured for separate shale sampled from the MIP-3H well.[49]

Measured VOCs in the LM-2 experiment were the highest out of all fluids sampled (Table 4 and Fig. 3A). VOCs were higher in both LM-2 and WV-7 compared to the HPT-HFF and below the detection limit in the MIP-3H experiment (Table 4 and Fig. 3A). The LM-2 sample contains a larger portion of labile hydrocarbons, as the OM within the shale has not been thermally degraded or altered to the same extent as the high maturity rocks.[21] Similar to the degradation of gelling agents, the labile portion of the organic macromolecules in shale subsequently transform and solubilize into fluid under high pressure and temperature as a result of kerogen reaction.[25] It has been shown that the persulfate breakers have been utilized to dissolve or breakdown the kerogen within subterranean formations (US Patent 2017/066959A1). Products of oxidizing breakers, such as ammonium persulfate, have been observed in produced water (*e.g.*, NH_4^+[50]). These residual breakers might react with kerogen in OM (for example, see ref. 25) and may potentially release these labile compounds over the life of the well. The absence of target VOCs in fluid from the MIP-3H experiment is likely a result of surface adsorption of VOCs to highly aromatic kerogen nanopores in the thermally mature shale.[24,51,52] The relatively high salinity of the produced fluid caused by the mixing of injection and formation fluids may increase the sorption of organic compounds onto activated carbon,[53] similar to what we observe for the highly mature kerogen of MIP-3H.

The molecular characteristics of the shale OM play a key role in controlling the organic composition of water produced from hydraulically fractured shale reservoirs and should be taken into consideration when assessing the environmental impact and recycling strategies associated with flowback and produced water. VOCs are commonly observed in both gaseous and solubilized forms around hydraulic fracturing operations and fluid-shale experiments.[3,8,54] Separators are effective in reducing some of the VOCs in the produced fluid, but some compounds remain in the fluids after separator treatment,[53] further demonstrating the need for understanding the source of these compounds and how they change over the life of the well.

5 Conclusions

Experiments were conducted to understand the inorganic and organic changes that occur in fracturing fluid and rock during the shut-in phase of HF operations. Experiments were carried out in high P–T autoclave reactors using samples of varying maturity and mineralogy from the Marcellus Shale. Our results indicate an increase of SO_4^{2-} and PO_4^{3-} ions and a decrease in Ba^{2+} ions in all shale–fluid reactions. The concentrations of these ions are controlled primarily by variations in shale mineralogy, especially by its carbonate and clay content. We also observed a net decrease in DOC (organic acids + NPOC) concentrations for all the shale–fluid reactions as compared to

the control HPT-HFF fluid. Further, we noted a decrease in concentrations of VOCs (benzene, toluene, and xylene) with increasing maturity, indicating adsorption of these organic species on shale OM.

The variations in chemical signatures of reacted fluids clearly suggest that the mineralogy and nature of OM play a key role in the mobilization of inorganic and organic components during HF operations. This also suggests that these reactions can vary significantly in different parts of the basin. Therefore, the chemical composition of HFFs should be modified to better target the varying mineralogical compositions and type of OM encountered in different parts of the basin. Further investigation on the sorption, transformation, transport, and fate of low molecular weight organic components in fluid–shale reactions is necessary to improve the understanding of geochemical reactions during hydraulic fracturing to optimize gas production, minimize environmental impact, and design water reuse and recycling strategies.

Conflicts of interest

There are no conflicts to declare.

Acknowledgements

Samples for this research were provided by SWN Energy, West Virginia Geological and Economic Survey, Northeast Natural Energy, and the Marcellus Shale Energy and Environment Laboratory (MSEEL) funded by the Department of Energy's National Energy Technology Laboratory (DOE-NETL) grants DE# FE0024297 and DE# FE0004000, and National Science Foundation grant (NSF DEB-1342732) to S. Sharma. Funding was also provided through the Department of Energy's Office of Oil and Natural Gas Unconventional Resources Research Program support of the NETL Research and Innovation Center's Onshore Unconventional Resources Portfolio.

References

1 U.S. EIA, *Updates to the Marcellus Shale Play Maps*, U.S. EIA, 2017, 14.
2 PA DEP, Hydraulic Fracturing Overview, http://files.dep.state.pa.us/OilGas/BOGM/BOGMPortalFiles/MarcellusShale/DEP%20Fracing%20overview.pdf.
3 S. J. Maguire-Boyle and A. R. Barron, *Environ. Sci.: Processes Impacts*, 2014, **16**, 2237–2248.
4 A. N. Paukert Vankeuren, J. A. Hakala, K. Jarvis and J. E. Moore, *Environ. Sci. Technol.*, 2017, **51**, 9391–9402.
5 A. L. Harrison, A. D. Jew, M. K. Dustin, D. L. Thomas, C. M. Joe-Wong, J. R. Bargar, N. Johnson, G. E. Brown and K. Maher, *Appl. Geochem.*, 2017, **82**, 47–62.
6 A. D. Jew, M. K. Dustin, A. L. Harrison, C. M. Joe-Wong, D. L. Thomas, K. Maher, G. E. Brown and J. R. Bargar, *Energy Fuels*, 2017, **31**, 3643–3658.
7 Q. Li, A. D. Jew, A. M. Kiss, A. Kohli, A. Alalli, A. R. Kovscek, M. D. Zoback, D. Cercone, K. Maher, G. E. J. Brown and J. R. Bargar, *Unconventional Resources Technology Conference*, 2018.
8 V. Marcon, C. Joseph, K. E. Carter, S. W. Hedges, C. L. Lopano, G. D. Guthrie and J. A. Hakala, *Appl. Geochem.*, 2017, **76**, 36–50.
9 T. T. Phan, A. N. Paukert Vankeuren and J. A. Hakala, *Int. J. Coal Geol.*, 2018, **191**, 95–111.
10 C. Strong Lisa, T. Gould, K. Lisa, J. Sadowsky Michael, A. Aksan and P. Wackett Lawrence, *J. Environ. Eng.*, 2014, **140**, B4013001.
11 K. Hoelzer, A. J. Sumner, O. Karatum, R. K. Nelson, B. D. Drollette, M. P. O'Connor, E. L. D'Ambro, G. J. Getzinger, P. L. Ferguson, C. M. Reddy, M. Elsner and D. L. Plata, *Environ. Sci. Technol.*, 2016, **50**, 8036–8048.
12 B. Ouyang, D. J. Renock, M. A. Ajemigbitse, K. V. Sice, N. R. Warner, J. D. Landis and X. Feng, *Environ. Sci.: Processes Impacts*, 2019, **21**, 339–351.
13 M. A. Ajemigbitse, F. S. Cannon, M. S. Klima, J. C. Furness, C. Wunz and N. R. Warner, *Environ. Sci.: Processes Impacts*, 2019, **21**, 308–323.
14 *Produced Water: Environmental Risks and Advances in Mitigation Technologies*, ed. K. Lee and J. Neff, Springer-Verlag, New York, 2011.
15 M. Elsner and K. Hoelzer, *Environ. Sci. Technol.*, 2016, **50**, 3290–3314.
16 A. J. Sumner and D. L. Plata, *Environ. Sci.: Processes Impacts*, 2018, **20**, 318–331.
17 N. Abualfaraj, P. L. Gurian and M. S. Olson, *Environ. Eng. Sci.*, 2014, **31**, 514–524.
18 FracFocus Chemical Disclosure Registry, http://fracfocus.org/, accessed 15 February 2019.
19 T. L. Tasker, P. K. Piotrowski, F. L. Dorman and W. D. Burgos, *Environ. Eng. Sci.*, 2016, **33**, 753–765.
20 V. Agrawal and S. Sharma, *Front. Energy Res.*, 2018, **6**, DOI: 10.3389/fenrg.2018.00042.
21 V. Agrawal and S. Sharma, *Fuel*, 2018, **228**, 429–437.
22 V. Agrawal, PhD thesis, West Virginia University, 2018.
23 V. Agrawal and S. Sharma, *Sci. Rep.*, 2018, **8**, 17465.
24 P. R. Craddock, T. V. Le Doan, K. Bake, M. Polyakov, A. M. Charsky and A. E. Pomerantz, *Energy Fuels*, 2015, **29**, 2197–2210.
25 M. K. Dustin, J. R. Bargar, A. D. Jew, A. L. Harrison, C. Joe-Wong, D. L. Thomas, G. E. Brown and K. Maher, *Energy Fuels*, 2018, **32**, 8966–8977.
26 R. Chen, S. Sharma, T. Bank, D. Soeder and H. Eastman, *Appl. Geochem.*, 2015, **60**, 59–71.
27 D. Jarvie and L. Lundell, *Hydrocarbon generation modeling of naturally and artificially matured Barnett shale, Ft. Worth Basin, Texas*, The Woodlands, Texas, 1991.
28 F. H. Chung, *J. Appl. Crystallogr.*, 1974, **7**, 519–525.
29 F. H. Chung, *J. Appl. Crystallogr.*, 1975, **8**, 17–19.
30 T. R. Malizia, *Geochemistry of the Marcellus Shale; Metals Mobility and Solubilization*, 2011.
31 P. Staub, *Clay Mineralogy of the Marcellus and Utica Shales: Implications for Fluid Development via Cation Exchange*, 2014.

32 D. Knetsch and W. L. Groeneveld, *Inorg. Chim. Acta*, 1973, **7**, 81–87.
33 J.-Y. Fang and C. Shang, *Environ. Sci. Technol.*, 2012, **46**, 8976–8983.
34 T. Phan, A. Hakala and D. Bain, *Appl. Geochem.*, 2018, **95**, 85–96.
35 F. D. H. Wilke, A. Vieth-Hillebrand, R. Naumann, J. Erzinger and B. Horsfield, *Appl. Geochem.*, 2015, **63**, 158–168.
36 M. Dieterich, B. Kutchko and A. Goodman, *Fuel*, 2016, **182**, 227–235.
37 D. Renock, J. D. Landis and M. Sharma, *Appl. Geochem.*, 2016, **65**, 73–86.
38 A. D. Jew, Q. Li, D. Cercone, K. Maher, G. E. J. Brown and J. R. Bargar, *Unconventional Resources Technology Conference*, 2018.
39 L. Wang, S. Burns, D. E. Giammar and J. D. Fortner, *Chemosphere*, 2016, **149**, 286–293.
40 J. Yang, M. Torres, J. McManus, T. J. Algeo, J. A. Hakala and C. Verba, *Chem. Geol.*, 2017, **466**, 533–544.
41 M. Blondes, K. Gans, M. Engle, Y. Kharaka, M. Reidy, V. Saraswathula, J. Thordsen, E. Rowan and E. Morrissey, *U.S. Geological Survey National Produced Waters Geochemical Database v2.3 (PROVISIONAL)*, USGS, 2017.
42 O. US EPA, Proceedings of the Technical Workshops for the Hydraulic Fracturing Study, https://www.epa.gov/hfstudy/proceedings-technical-workshops-hydraulic-fracturing-study-chemical-and-analytical-methods, accessed 15 February 2019.
43 R. Pal, *ARKIVOC*, 2018, **2018**, 346–371.
44 S. Zargari, K. L. Canter and M. Prasad, *Fuel*, 2015, **153**, 110–117.
45 T. Zhang, G. S. Ellis, S. C. Ruppel, K. Milliken and R. Yang, *Org. Geochem.*, 2012, **47**, 120–131.
46 B. Xiong, Z. Miller, S. Roman-White, T. Tasker, B. Farina, B. Piechowicz, W. D. Burgos, P. Joshi, L. Zhu, C. A. Gorski, A. L. Zydney and M. Kumar, *Environ. Sci. Technol.*, 2018, **52**, 327–336.
47 Y. Zhu, A. Vieth-Hillebrand, F. D. H. Wilke and B. Horsfield, *Int. J. Coal Geol.*, 2015, **150–151**, 265–275.
48 T. I. Eglinton, C. D. Curtis and S. J. Rowland, *Mineral. Mag.*, 1987, **51**, 495–503.
49 J. A. Hakala, T. Phan, M. Stuckman, H. Edenborn and C. Lopano, Role of Organic Acids in Controlling Mineral Scale Formation During Hydraulic Fracturing at the Marcellus Shale Energy and Environmental Laboratory (MSEEL) Site, *Unconventional Resources Technology Conference*, Austin, Texas, USA, 2017, DOI: 10.15530/URTEC-2017-2670833.
50 J. S. Harkness, G. S. Dwyer, N. R. Warner, K. M. Parker, W. A. Mitch and A. Vengosh, *Environ. Sci. Technol.*, 2015, **49**, 1955–1963.
51 V. Agrawal and S. Sharma, *Sci. Rep.*, 2019, (in review).
52 G. Cornelissen, Ö. Gustafsson, T. D. Bucheli, M. T. O. Jonker, A. A. Koelmans and P. C. M. van Noort, *Environ. Sci. Technol.*, 2005, **39**, 6881–6895.
53 A. Butkovskyi, H. Bruning, S. A. E. Kools, H. H. M. Rijnaarts and A. P. Van Wezel, *Environ. Sci. Technol.*, 2017, **51**, 4740–4754.
54 W. Orem, C. Tatu, M. Varonka, H. Lerch, A. Bates, M. Engle, L. Crosby and J. McIntosh, *Int. J. Coal Geol.*, 2014, **126**, 20–31.